END

FILMED

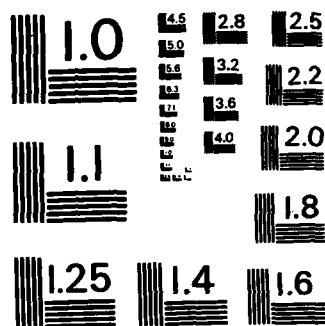DTIC

MICROCOPY RESOLUTION TEST CHART
NATIONAL BUREAU OF STANDARDS-1963-A

X-Ray Lines of Helium-Like
Oxygen and Neon in the Solar Corona

D. L. McKENZIE and P. B. LANDECKER
Space Sciences Laboratory
Laboratory Operations
The Aerospace Corporation
El Segundo, Calif. 90245

30 September 1982
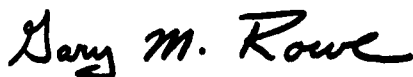
DTIC
ELECTE
NOV 15 1982

A

Prepared for

This report was submitted by The Aerospace Corporation, El Segundo, CA 90245, under Contract No. F04701-81-C-0082 with the Space Division, Deputy for Technology, P.O. Box 92960, Worldway Postal Center, Los Angeles, CA 90009. It was reviewed and approved for The Aerospace Corporation by H. R. Rugge, Director, Space Sciences Laboratory. Captain Gary M. Rowe, SD/YLT, was the project officer for the Mission-Oriented Investigation and Experimentation (MOIE) Program.

This report has been reviewed by the Public Affairs Office (PAS) and is releasable to the National Technical Information Service (NTIS). At NTIS, it will be available to the general public, including foreign nations.

This technical report has been reviewed and is approved for publication. Publication of this report does not constitute Air Force approval of the report's findings or conclusions. It is published only for the exchange and stimulation of ideas.
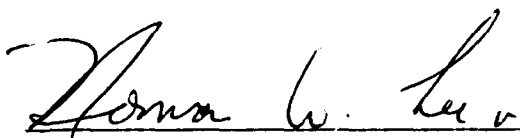

Gary M. Rowe, Captain, USAF
Project Officer

Jimmie H. Butler, Colonel, USAF
Director of Space Systems Technology

FOR THE COMMANDER

Norman W. Lee, Jr., Colonel, USAF
Deputy for Technology

REPORT DOCUMENTATION PAGE		READ INSTRUCTIONS BEFORE COMPLETING FORM
1. REPORT NUMBER SD-TR-82-85	2. GOVT ACCESSION NO. ADA	3. RECIPIENT'S CATALOG NUMBER
4. TITLE *(and Subtitle)* X-RAY LINES OF HELIUM-LIKE OXYGEN AND NEON IN THE SOLAR CORONA		5. TYPE OF REPORT & PERIOD COVERED
		6. PERFORMING ORG. REPORT NUMBER TR-0082(2940-01)-7
7. AUTHOR(s) D. L. McKenzie and P. B. Landecker		8. CONTRACT OR GRANT NUMBER(s) F04701-81-C-0082
9. PERFORMING ORGANIZATION NAME AND ADDRESS The Aerospace Corporation El Segundo, Calif. 90245		10. PROGRAM ELEMENT, PROJECT, TASK AREA & WORK UNIT NUMBERS
11. CONTROLLING OFFICE NAME AND ADDRESS Space Division Air Force Systems Command Los Angeles, Calif. 90009		12. REPORT DATE 30 September 1982
		13. NUMBER OF PAGES 35
14. MONITORING AGENCY NAME & ADDRESS(if different from Controlling Office)		15. SECURITY CLASS. *(of this report)* Unclassified
		15a. DECLASSIFICATION/DOWNGRADING SCHEDULE

16. DISTRIBUTION STATEMENT *(of this Report)*

Approved for public release; distribution unlimited.

17. DISTRIBUTION STATEMENT *(of the abstract entered in Block 20, if different from Report)*

18. SUPPLEMENTARY NOTES

19. KEY WORDS *(Continue on reverse side if necessary and identify by block number)*

Sun:corona
Sun:flares
Sun:spectra
Sun:X-rays

20. ABSTRACT *(Continue on reverse side if necessary and identify by block number)*

Line ratios from the helium-like ions O VII and Ne IX are useful as plasma diagnostics for both flaring and nonflaring solar coronal active regions. The photon flux ratio, R, of the forbidden $1s^2 \, ^1S_0 - 1s2s \, ^3S_1$ line to the intercombination $1s^2 \, ^1S_0 - 1s2p \, ^3P_1$ line in O VII is useful as a density diagnostic at coronal temperatures of $\sim 2 \times 10^6$ K. If the electron density n_e is less than $n_e^* \sim 3 \times 10^9$ cm^{-3}, $R \approx R_0$ (where R_0 is the low-density limit), and R decreases with increasing density. Uncertainties in R and R_0 both

19. KEY WORDS (Continued)

20. ABSTRACT (Continued)

contribute to uncertainties in n_e. R uncertainties are especially important
for nonflaring plasmas having $n_e \approx n_e^*$. We analyzed 29 nonflare solar X-ray
spectra, each a sum of ~ 10 scans by the SOLEX B spectrometer on the U.S.A.F.
P78-1 satellite, to conclude that R_0 is in the range 3.7–4.1. G, the photon
flux ratio of the forbidden plus intercombination line to the resonance
$1s^2 \; {}^1S_0 - 1s2p \; {}^1P_1$ line, can be used as an indicator of whether or not the
emitting plasma is in a state of ionization equilibrium. For both O VII and
Ne IX, G is modified by resonance scattering in the solar atmosphere, which
lowers the resonance line flux. This scattering allows us to estimate the
column densities of O VII and Ne IX in the corona above the active region
source. We also estimate G_0, the value of G in the absence of resonance
scattering. We find G_0(O VII) ≈ 1.0 and G_0(Ne IX) ≈ 0.8. In the relatively
few flares we have analyzed we find no evidence of a departure from ioniza-
tion equilibrium.

$* \; R \qquad (\text{...} \qquad \text{(photon...} \\ \qquad\qquad \text{forbid. line)}$

PREFACE

We thank S. Painter and J. Washington for reducing the SOLEX data.

Accession For

NTIS GRA&I	☑
D?IC TAB	☐
Unannounced	☐
Justification	

Distribution/

Availability Codes

1

CONTENTS

FIGURES

TABLES

I. INTRODUCTION

The study of the active solar corona requires information about such thermodynamic variables as the plasma temperature, density, and pressure as a function of position. X-ray spectra allow the distribution of emission measure $\int n_e^2 dV$ as a function of temperature to be determined in flaring (McKenzie and Landecker 1981) and nonflaring active regions. V is the volume and n_e the electron density. The usefulness of the emission measure is limited because n_e appears in the second power. In general, such quantities as the electron density, n_e, or the pressure, $n_e kT$, cannot be derived from emission measure alone. A direct measurement of n_e is required.

A small number of density-diagnostic X-ray line ratios are available. Gabriel and Jordan (1969) showed that the flux ratio, R, of the $1s^2 \, ^1S_0 - 1s2s \, ^3S_1$ forbidden line to the $1s^2 \, ^1S_0 - 1s2p \, ^3P_1$ intercombination line in the helium-like ions would be density-sensitive for densities exceeding a species-dependent lower limit n_e^* (in this paper we consider flux ratios where flux density has units of photons $cm^{-2} \, s^{-1}$). The ratio in O VII (McKenzie et al. 1980a; Doschek et al. 1981) has been used to derive coronal densities in solar flares. R for Ne IX, Mg XI, and Si XIII may also prove to be useful, but for ions heavier than these n_e^* is almost certainly larger than n_e ever gets in the corona. In addition, a line ratio in Fe XXI (Mason et al. 1979) provides a density diagnostic for $n_e > 10^{12} \, cm^{-3}$. McKenzie and Landecker (1982) have shown that the same ratio in Ca XV is useful for measuring densities that are commonly present in flares at tempera-

tures of $\sim 4 \times 10^6$ K. The Fe XXI diagnostic has not yet been used because at $\sim 10^7$ K, the temperature at which Fe XXI is most abundant, densities are apparently rarely high enough to yield a measurable effect (McKenzie et al. 1980b).

The O VII density diagnostic is especially interesting because it offers the capability of measuring n_e in at least some nonflaring active regions. The O VII lines are produced at $\sim 2 \times 10^6$ K, in the range of temperatures commonly observed in coronal active regions. Furthermore n_e^*(O VII) $\approx 3 \times 10^9$ cm^{-3}, a density that is sometimes exceeded in the nonflaring corona. A major aim of the present paper is to examine the usefulness of the O VII ratio in the nonflaring corona. To do this we analyze data from the SOLEX B spectrometer aboard the U. S. Air Force P78-1 satellite (Landecker, McKenzie, and Rugge 1979; McKenzie et al. 1980b). The resolving power of the spectrometer is not high enough to permit a similar study of R for Ne IX.

The helium-like line ratio,

$$G = \frac{F(1s^2\ {}^1S_0 - 1s2s\ {}^3S_1) + F(1s^2\ {}^1S_0 - 1s2p\ {}^3P_1)}{F(1s^2\ {}^1S_0 - 1s2p\ {}^1P_1)} , \qquad (1)$$

where F is flux, is useful as an indicator of the state of ionization equilibrium during flares (Acton and Brown 1978; see also Gabriel and Jordan 1969, note added in proof). In addition the resonance line (denominator) is depleted by resonance scattering in the corona (Acton 1978), so G can be used as a measure of the coronal column density of O VII. For O VII the resonance line is most strongly emitted at temp-

10

erature $T \sim 2 \times 10^6$ K, but the population of the absorbing O VII ions is highest at $\sim 1 \times 10^6$ K (Jacobs et al. 1978). Thus G can be used as a probe of the quiet corona between the observer and the emitting active region. The spectra of both O VII and Ne IX show resonance scattering effects. We examine G as a plasma diagnostic for both species in § III.

II. THE O VII DENSITY DIAGNOSTIC

The electron density in a 2×10^6 K plasma can be derived from the ratio R for O VII as follows (Pradhan and Shull 1981):

$$n_e = 3.1 \times 10^{10} \left(\frac{R_o}{R} - 1\right) \text{cm}^{-3} . \qquad (2)$$

R_o is the value taken by R in the limit of low densities. It is customary to assume that densities for which $R_o/R - 1 > 0.1$ are measurable (Gabriel and Jordan 1969), but this may not always be true since statistical errors in R and uncertainties in R_o both contribute to the error in n_e. Differentiating equation (2), we find

$$\frac{\partial n_e}{\partial R_o} = \frac{3.1 \times 10^{10}}{R} \text{cm}^{-3} . \qquad (3)$$

Even if statistical uncertainties in R are negligible, for active region densities of a few times 10^9 cm^{-3}, a 10% uncertainty in R_o can result in very large errors in the derived n_e. Obtaining an accurate value for R_o is of primary importance in applying the density diagnostic to nonflaring plasmas.

11

Gabriel and Jordan (1972) calculated, for O VII, $R_O = 3.6$, and this value has largely been accepted ever since. More recently Pradhan and his colleagues have recalculated R_O taking into account autoionizing resonances in the collisional excitation cross sections (Pradhan, Norcross, and Hummer 1981; Pradhan and Shull 1981). Pradhan and Shull find R_O(O VII) $= 3.95$. They estimate that the overall error in their line ratios (for a number of helium-like ions) should not exceed 25%, but recently Pradhan (1981) has estimated that the errors for ions other than Fe XXV and Ca XIX ("particularly O VII") should be "well below 10%."

Prior to the P78-1 launch on 1979 February 24, a substantial data set of R(O VII) measurements existed. Rugge and Walker (1970, 1971) compiled data from the OV1-10 satellite for 90 days in 1966/1967 and from the OV1-17 satellite for a few days in 1969. They found mean values, $\overline{R}$, of 3.3 and 3.2, respectively, in the two data sets. The data can be criticized in that the spectral resolution, particularly in the OV1-10 data, does not allow the resonance and intercombination lines to be resolved well, and the background in the relevant wavelength region is consequently difficult to estimate. Substantial systematic errors may be in effect. Acton et al. (1972) and Acton and Catura (1976) report measurements of R(O VII) by rocket-borne spectrometers with much better spectral resolution. In each case the ratios are distributed about a mean of ~ 3.6. The Acton-Catura (1976) data include one region in which $\overline{R}/R = 1.25$. The authors interpret this as a positive measurement of the density. Furthermore, they point out

12

that, as a result of the co-existence in the spectrometer field-of-view of high- and low-density regions, the $\overline{R}$ value of 3.60 was below the low-density limit value, R_o. One measurement by Acton et al. (1972) and one by McKenzie et al. (1978) are of particular interest in that active regions were excluded from the respective fields of view. The values of R from these measurements should be close to R_o. Acton et al. (1972) found R = 3.4 ± 0.1 and McKenzie et al. (1978) found R = 4.2 ± 0.2. The former value is surprisingly low; in fact it is lower than or equal to R in all six active regions or complexes of active regions reported in the same paper. Perhaps undetected dense material was within the field of view. The McKenzie et al. (1978) result is consistent with the Pradhan and Shull (1981) value of R_o but not with that of Gabriel and Jordan (1972).

In summary, theoretical values of R_o range from 3.6 to 3.95, the latter value arising from more recent and sophisticated calculations. Observations of nonflaring plasmas have yielded values of R from ~ 3.2 to ~ 4.2. The best of the rocket observations appear to be those of Acton and Catura (1976), which combine high counting rates with spectral resolution adequate to resolve the three O VII lines. The McKenzie et al. (1978) result comes close to being a direct measurement of R_o and combines high counting rates with adequate spectral resolution (somewhat worse than that of Acton and Catura (1976)). Both the Acton-Catura and McKenzie et al. results support R_o > 3.60.

The SOLEX B data set to be considered here consists of 29 measurements of R (and G) made between 1979 April 5 and July 22. Each

13

measurement uses data from a sum of ~ 10 successive spectral scans. Individual spectral scans take either 84 s or 168 s to traverse the Bragg angle range of 17.4° - 61.7° in 30".2 steps. The spectrometer is collimated to a 60" (FWHM) square field of view, and in these measurements a rubidium acid phthalate crystal (RAP; 2d = 26.121 Å) was used. With possible exceptions to be discussed below, the spectra are of nonflaring active regions, but the collimator restricts the field of view so that the brightest or densest parts of the regions are not always viewed. The O VII lines are barely detectable outside active regions. Figure 1 shows two sample (slow scan) O VII summed spectra. The spectra are comparable to the Acton and Catura (1976) rocket measurements in both spectral resolution and counting statistics. The forbidden line integrated count less background is typically several thousand. The SOLEX spectra have the advantage of finer collimation than the 1.3' one-dimensional collimator used in the Acton-Catura observations.

We first attempted to fit the SOLEX data in the wavelength range shown in Figure 1 to a model consisting of the continuum and seven spectral lines: the three O VII lines, the Ca XVI 2p $^2P_{1/2}$ - 3d $^2D_{3/2}$ line at 21.444 Å (McKenzie and Landecker 1982), and three unidentified weak lines at 22.03 Å, 21.94 Å, and 21.97 Å. The last two lines mentioned were marginally detected in flare spectra; they had a negligible effect on the fits. The background was fitted using a two-parameter fit which was linear in the calculated spectrometer sensitivity as a function of wavelength. A Voigt line profile was used
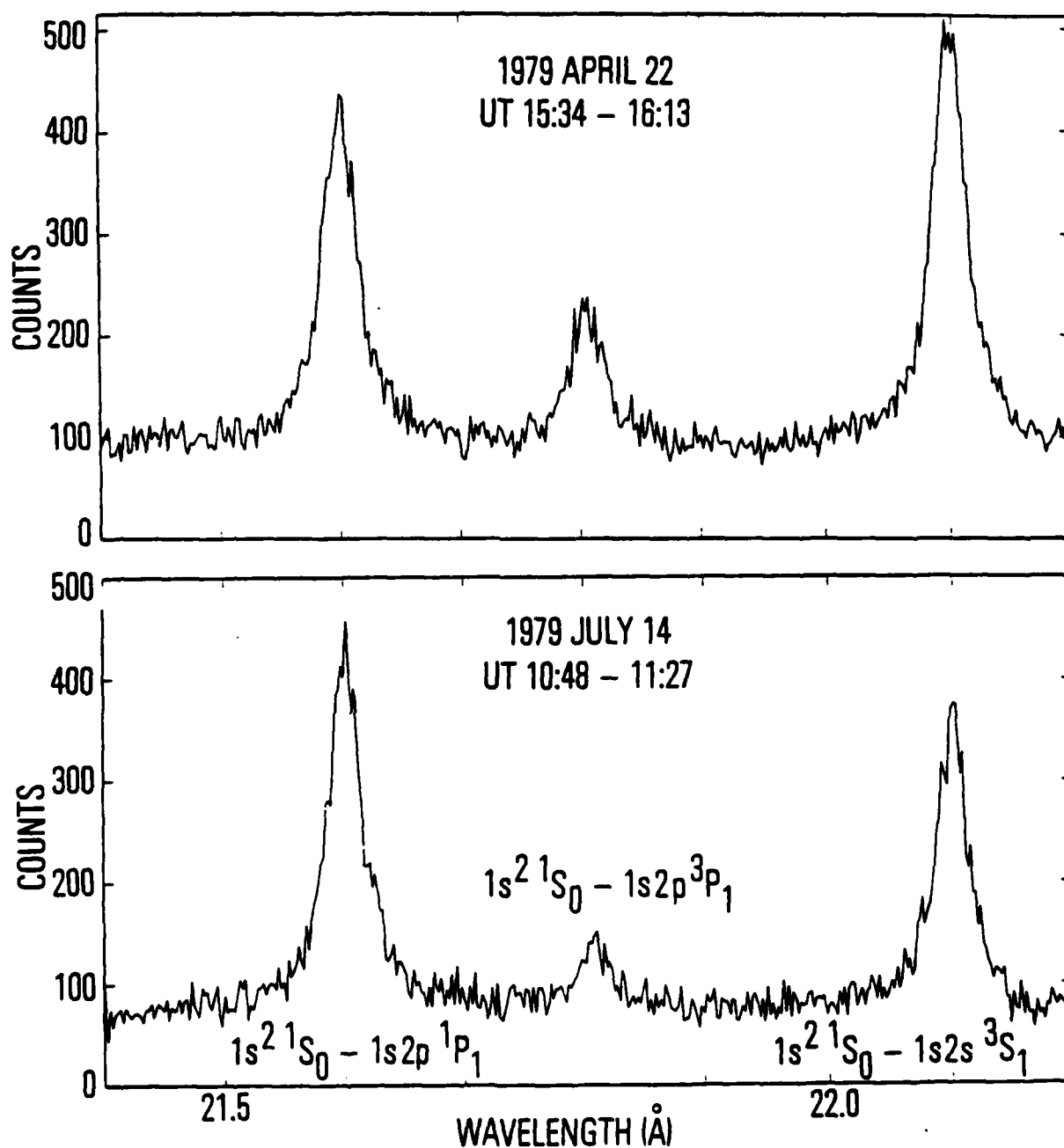
14

Figure 1. X-Ray Spectra of Two Solar Active Regions Showing Strong
Lines of O VII. The spectra were chosen to illustrate
the variability in the data. The upper spectrum has
R ≈ 3.4 and G ≈ 1.8, while the lower has R ≈ 3.9 and
G ≈ 1.2.

15

(Finn and Mugglestone 1965) with the line positions and widths as free parameters. In only ten of the 27 spectra fitted using a minimum-χ^2 criterion was the χ^2 acceptable at the 95% χ^2 probability level (with 442 degrees of freedom, $\chi^2 < 491$ was acceptable). We attribute this failure to difficulty in modeling the line profiles of the strong O VII lines. Resonance scattering effects, to be discussed in § III, can significantly distort the resonance line profile, especially near line center.

Since the results from the spectral fits were unsatisfactory, we used another method to determine R. The counts under each line were summed over 40 spectrometer steps (20.1') and the sums were corrected for background; the background obtained from the spectral fits was used. Then each sum was corrected to a full line sum, where we assumed the profiles were Lorentzian in the wings. This is a good assumption since the line shape in the wings is dominated by the instrumental profile, which is approximately Lorentzian. The corrections to the intercombination and forbidden line sums resulting from this process were, respectively, 1.011 and 1.028 times the resonance line correction. The line profiles are of such width that the resonance and forbidden lines make small contributions to the intercombination line fluxes. Therefore, 1.09% of the corrected resonance line count and 0.54% of the corrected forbidden line count were subtracted from the corrected intercombination line count. Finally, each sum was corrected for spectrometer response as a function of wavelength and R was calculated. The results are shown in Table 1 (R_{SUM}). We also

16

TABLE 1

R for O VII

Spectrum Number	Date (1979) Mo.-Day	UT	McMath Plage	R_{SUM}	R_{FIT}	n_e (10^9 cm^{-3})
1	4-5	19:17	15918	3.76 ± 0.17	3.78 ± 0.17	
2	4-6	22:37	15918	3.46 ± 0.16	3.30 ± 0.14	3.9 ± 2.4
3	4-20	10:55	15942	3.76 ± 0.23	3.74 ± 0.18	
4	4-21	15:49	15942	3.58 ± 0.19	3.55 ± 0.18	
5	4-22	15:53	15942	3.44 ± 0.12	3.36 ± 0.14	4.1 ± 2.2
6	5-2	19:54	15974	3.69 ± 0.18	3.68 ± 0.16	
7	5-4	10:28	15974	4.18 ± 0.35	4.06 ± 0.32	
8F	6-6	02:48	16051	3.71 ± 0.31		
9F	6-6	13:17	16051	a		
10F	6-7	12:53	16051	2.73 ± 0.34		13.3 ± 6.0
11F	6-8	07:00	16051	3.45 ± 0.23		4.0 ± 2.9
12F	6-9	03:52	16051	3.97 ± 0.22		
13F	6-10	11:31	16051	4.06 ± 0.41	3.81 ± 0.37	
14F	6-11	03:34	16051	4.38 ± 0.30		
15F	6-11	16:25	16051	3.11 ± 0.36		7.9 ± 4.9

17

TABLE 1 (Con't)

R for O VII

Spectrum Number	Date (1979) Mo.-Day	UT	McMath Plage	R_{SUM}	R_{FIT}	n_e (10^9 cm^{-3})
16F	6-12	13:16	16051	3.75 ± 0.34		
17	6-13	07:09	16051	3.78 ± 0.15	3.72 ± 0.15	
18	7-8	12:13	16117	3.84 ± 0.17		
19	7-9	07:26	16117	3.74 ± 0.12	3.71 ± 0.10	
20	7-10	23:39	16117	3.85 ± 0.10		
21	7-11	18:51	16117	3.85 ± 0.13		
22	7-12	07:46	16122	3.73 ± 0.14		
23	7-13	15:49	16122	3.44 ± 0.11		4.1 ± 2.1
24	7-14	11:07	16137	3.88 ± 0.19		
25	7-16	11:15	16137	3.71 ± 0.17		
26	7-17	09:40	16137	3.34 ± 0.18		5.2 ± 2.7
27	7-19	06:39	16137	3.82 ± 0.28		
28	7-21	16:23	16160	2.97 ± 0.10		9.7 ± 2.8
29	7-22	06:50	16160	3.48 ± 0.10		3.7 ± 2.0
30	7-22	19:43	16160	3.53 ± 0.13		3.2 ± 2.2

[a] O VII data not usable.

show R from the spectral fitting program, where acceptable fits were obtained. "F" beside the spectrum number indicates that the fast stepping rate was used.

It is difficult to establish with certainty that no flare was in progress at a given time. We have used published flare listings and measurements by the MONEX low-energy X-ray monitor, also on P78-1, to check for possible flares. There were reported subflares in the observed regions near the observation times for spectra 6, 22, and 28, and possible minor bursts detected by the MONEX experiment, which views the whole solar disk, for numbers 24 and 29. These possible flares will not affect the conclusions below, but, at least in the case of spectrum 28, it is doubtful that nonflare densities were measured.

If the data are weighted by σ^{-2}, $\overline{R}$, the mean value of R from Table 1, is 3.59 but the distribution of measurements is not consistent with the assumption that R_0 is 3.59 and all observed regions are in the low-density limit. Low R values can be explained as arising from high-density regions, but high values of R cannot be similarly eliminated. By eliminating all observations having R more than 2σ below 3.59 (spectra 10, 28), where σ is the tabulated standard deviation, we arrived at $\overline{R}$ = 3.66, but the distribution was still inconsistent with R_0 = $\overline{R}$. Finally, by eliminating all observations for which R + 2σ < 3.75 (spectra 5, 10, 23, 26, 28, and 29), we find that $\overline{R}$ = 3.74 and that the distribution is consistent with $\overline{R}$ = R_0 with all remaining observations being in the low-density limit. Of course,

higher values of R_o are also possible if some of the observations are of regions having densities above $\sim 3 \times 10^9$ cm^{-3}. Actually R_o increases slowly with increasing temperature, as Blumenthal, Drake, and Tucker (1972) pointed out. Pradhan and Shull (1981) predict a slower increase than did these authors. The value 3.95 pertains to T = T_m = 1.87×10^6 K (the temperature of maximum O VII population), which is probably close to the average temperature in the active regions we observed. The densities in Table 1 are derived under the assumption that R_o = 3.9 ± 0.2. Our measurements are not corrected for satellite lines. Bhalla, Gabriel, and Presnyakov (1975) give the satellite line strengths relative to the resonance line strength, which itself includes unresolved satellite lines. In our data analysis procedure, satellite lines increase the apparent forbidden line flux by 2.0% of the resonance line flux and the intercombination line flux by 0.3% of the resonance line flux at T = T_m. For T > T_m the effect is smaller. The net result is that the measured R is increased by $\sim$ 1% at T = T_m.

III. G, THE TRIPLET-TO-SINGLET LINE RATIO

Acton and Brown (1978) showed that the ratio G, defined in equation (1), can be useful as an indicator of the state of ionization equilibrium. All three upper levels involved in G are populated by recombination, but the triplets are affected more than the singlet. In a recombining plasma, where the O VIII population is higher than would be expected from the electron temperature, G is higher than its

20

ionization equilibrium value. Conversely, G is lower in an ionizing plasma. Unfortunately, because of degradation of the resonance line flux by resonance scattering, a single measurement of G is inadequate to determine the state of ionization equilibrium for the case of a recombining plasma. Resonance scattering significantly affects G for both O VII and Ne IX.

Acton (1978) has applied resonance scattering theory to the coronal helium-like ions. The process consists of the absorption of a photon by an ion in the $1s^2\ ^1S_0$ ground state to produce an excited ion in the $1s2p\ ^1P_1$ state, which then decays to the ground state. In our observations of active regions, the following processes generate or alter the detected X-ray flux: emission in the active region, scattering of X-rays emitted by the active region into the detector, and scattering of radiation out of the beam headed for the detector. Detection, either directly or after scattering, of X-rays emitted outside active regions is negligible. This is verified by the fact that O VII and Ne IX lines are measurable by the SOLEX B spectrometer only when an active region is in the field of view.

Observations from Skylab made it obvious that the corona is highly structured. Interpretations of the observations have led to the idea that nearly all the coronal plasma is confined in closed magnetic flux tubes (Rosner, Tucker and Vaiana 1978; Serio et al. 1981). Recently Pallavicini et al. (1981) found that the observed properties of a wide variety of loops within and interconnecting active regions can be reproduced satisfactorily with simple static

21

loop models. The old model of a uniform atmosphere in hydrostatic equilibrium is replaced by an ensemble of loops, each in hydrostatic equilibrium. In looking at active region emission we are looking through a collection of loops. The optical depth, τ, is proportional to path length, given by $\Delta r s(\theta)$, where

$$s(\theta) = (\frac{r_s}{\Delta r}) \cos\theta \left\{ \left[1 + \sec^2\theta \left(\frac{2\Delta r}{r_s} + (\frac{\Delta r}{r_s})^2 \right) \right]^{\frac{1}{2}} - 1 \right\}. \qquad (4)$$

In equation (4), θ is the angle between the line of sight and the inward normal to the solar surface, r_s is the solar radius, and Δr is the thickness of the shell in which the scattering occurs. When $2\Delta r \sec^2\theta/r_s \ll 1$, $s(\theta) \approx \sec\theta$; that is, a plane atmosphere is a good approximation. Equation (4) is not valid for $\theta > 90°$, and for $\theta \approx 90°$ the collimator field of view is large enough that θ is poorly defined so the equation should not be used. Because of the nonuniform structure mentioned above, the relationship between τ and $s(\theta)$ is expected to show considerable scatter.

An active region emits resonance line radiation toward the detector both directly and by scattering. The scattering component is small because the optical thickness of the active region is small. We estimate that scattering accounts for $\le$ 5% of the resonance line flux emanating from an active region and assume that this fraction does not vary with angle. The estimate is based on analysis to be discussed later in this section.

22

In order for an X-ray to be scattered into the detector, the scattering must take place within the field of view and the final propagation direction must be within the very small detector solid angle. Scattering _into_ the detector becomes less important as the angle θ increases. To see this, consider a scattering element of volume dV in the "quiet corona" at a height z above an emitting point P, such that the vector from P to dV makes an angle θ' with the local vertical. The solid angle subtended by dV at P, and therefore the flux through dV, is proportional to $(z\sec\theta')^{-2}$. The probability of a scattering occurring in the height range z to z + dz is $\kappa dz\sec\theta'$, where κ is the resonance scattering "absorption coefficient." Thus the number of scatterings toward the detector per unit z-range is proportional to $\cos\theta'$. Since active regions and the detector field of view both have characteristic sizes in the arc minute range (1 arc min = 4×10^9 cm), θ' takes on a wide range of values, but the average value increases with θ. Thus scattering into the detector decreases with increasing θ.

If scattering into the detector is negligible compared to scattering out, the resonance line flux, F_r, is proportional to $e^{-\tau}$, where τ is the optical depth. Then, for θ not near 90°,

$$\frac{G}{G_o} \sim F_r^{-1} \sim e^{\tau} = \exp[s(\theta) \int_{z_s}^{\infty} \kappa(z)dz], \qquad (5)$$

where z_s is the height of the source in the corona, G_o is the value G would take were resonance scattering negligible, and $\kappa(z)$ is the

23

average "absorption coefficient" integrated over the line profile, taking into account the temperatures of both the emitting and absorbing regions. Equation (5) does not take into account changes in the line shape caused by absorption, but such changes can be neglected if $\tau < 1$, as it is here. Taking the natural logarithm of equation (5) we have

$$\ln G \approx [\int_{z_s}^{\infty} \kappa(z)dz]s(\theta) + \ln G_o. \tag{6}$$

For $\theta \approx 0$, scattering into the detector may be comparable in importance to scattering out, with the relationship depending on the geometry of the emitting region and the detector field of view. Scattering in becomes less important with increasing θ, and equation (6) is a useful approximation for determining the column density of material along the line of sight.

Table 2 gives the measured values of G for both O VII and Ne IX. The spectrum numbers are the same as in Table 1. We derived the G values for O VII by using the summing technique in §II. For Ne IX the technique differed in that each initial sum was over 30 (not 40) spectrometer steps, and the background was interpolated from counting rates in two spectral ranges (shaded in Figure 2). Figure 2 shows the spectrum around the Ne IX lines. The Ne IX intercombination line is near the resonance line and is much weaker. This prevents a good R determination for Ne IX, but since G is near 1.0, corrections to the intercombination line are relatively unimportant in determining G.

24

TABLE 2

G for O VII and Ne IX

Spectrum Number	θ (degrees)	s(θ)	G(O VII)	G(Ne IX)
1	44	1.36	1.17 ± 0.03	0.78 ± 0.02
2	58	1.75	1.19 ± 0.03	0.80 ± 0.03
3	54	1.62	1.36 ± 0.04	0.89 ± 0.04
4	66	2.14	1.82 ± 0.05	0.89 ± 0.03
5	74	2.86	1.84 ± 0.04	0.92 ± 0.02
6	19	1.06	1.01 ± 0.02	0.77 ± 0.05
7	33	1.18	1.01 ± 0.03	0.91 ± 0.06
8F	19	1.06	1.08 ± 0.04	0.81 ± 0.04
9F	19	1.06	a	0.81 ± 0.03
10F	23	1.08	1.14 ± 0.07	0.82 ± 0.08
11F	32	1.17	1.09 ± 0.03	0.84 ± 0.04
12F	42	1.31	1.21 ± 0.03	0.87 ± 0.04
13F	57	1.73	1.00 ± 0.04	0.86 ± 0.06
14F	64	2.04	1.24 ± 0.04	0.72 ± 0.05
15F	70	2.47	1.54 ± 0.09	0.90 ± 0.09
16F	82	3.94	1.78 ± 0.08	1.09 ± 0.11
17	92		1.93 ± 0.03	0.98 ± 0.05
18	58	1.75	1.47 ± 0.03	0.91 ± 0.05
19	68	2.30	1.60 ± 0.03	a
20	92		2.25 ± 0.04	0.99 ± 0.04
21	101		2.01 ± 0.04	0.90 ± 0.05
22	57	1.72	1.45 ± 0.03	1.07 ± 0.04
23	74	2.87	2.25 ± 0.05	1.01 ± 0.04

25

TABLE 2 (Con't)

G for O VII and Ne IX

Spectrum Number	θ (degrees)	$s(\theta)$	G(O VII)	G(Ne IX)
24	48	1.46	1.21 ± 0.03	0.82 ± 0.04
25	33	1.18	1.27 ± 0.03	0.77 ± 0.04
26	31	1.15	1.20 ± 0.03	0.65 ± 0.06
27	38	1.25	1.16 ± 0.04	0.85 ± 0.08
28	64	2.05	1.43 ± 0.03	b
29	71	2.54	1.65 ± 0.03	1.00 ± 0.03
30	77	3.20	1.87 ± 0.04	0.92 ± 0.03

[a]Data not usable.
[b]Probable flare, possible Fe XIX emission.
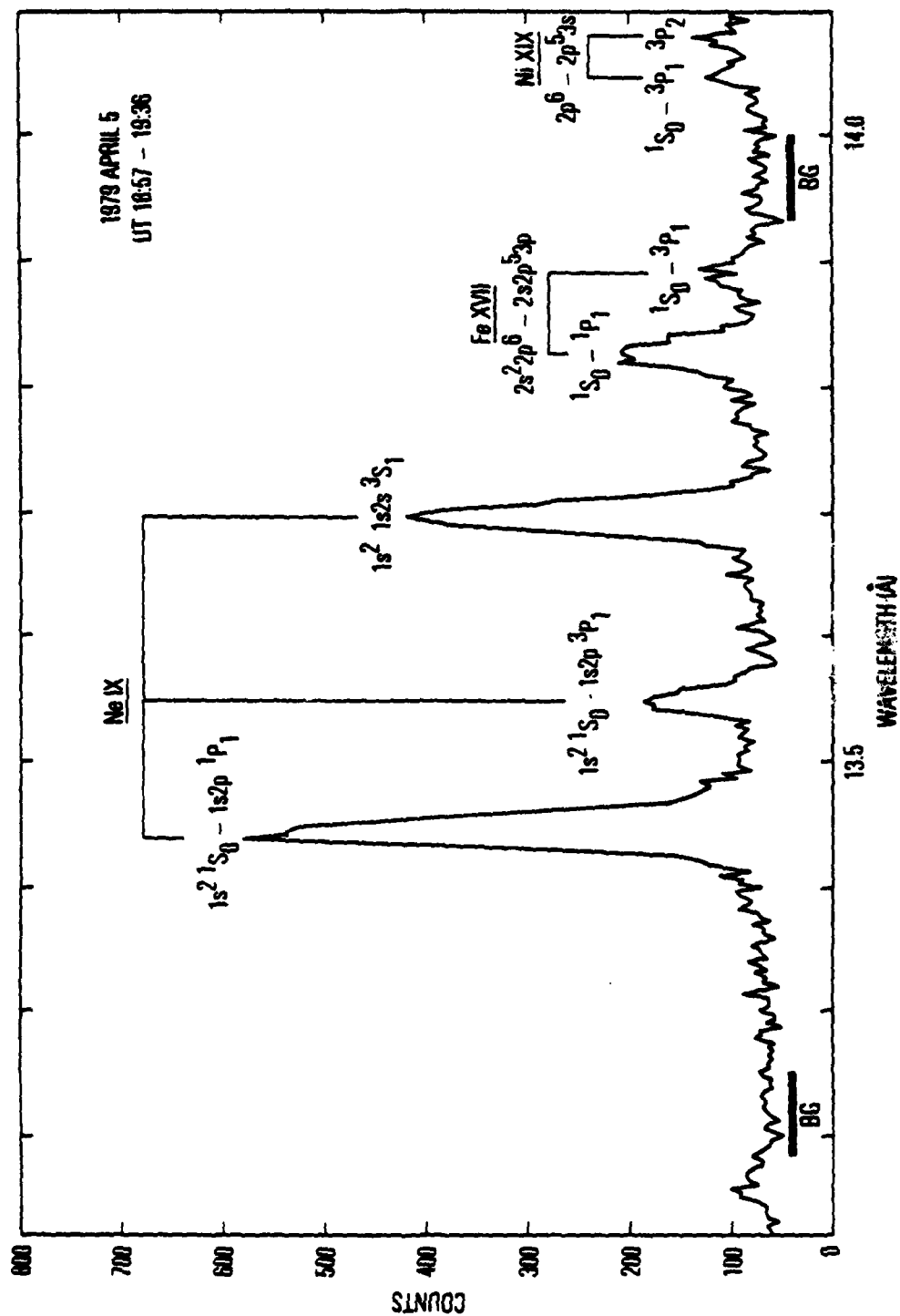
Figure 2. X-ray Spectrum of an active Region Showing Ne IX Emission Lines. The regions in which background was measured are shaded.

For Ne IX such corrections lower G by 0.059, and for O VII G is lowered by 0.015. Errors in G associated with the line shape will be smaller than these corrections. The G values are not corrected for satellite lines. It is customary to include blended satellite lines in theoretical calculations of G (Acton and Brown 1978; Pradhan and Shull 1981). The calculations therefore correspond to the line ratio that is actually observed, and direct comparisons between theory and observation are facilitated. For Ne IX there is also the possibility of a blend with Fe XIX lines. The Fe XIX population peaks at $T \approx 7 \times 10^6$ K and is small below $\sim 4 \times 10^6$ K (Jacobs et al. 1977). Therefore, we expect Fe XIX emission from nonflaring plasmas to be weak. We have not found any evidence of its existence. The strongest Fe XIX lines are blended with the weak Ne IX intercombination line in our flare spectra (Bromage and Fawcett 1977; McKenzie et al. 1980b), so Fe XIX emission should be manifested by a decrease in the ratio of forbidden to intercombination line counts. Thus if the measured G has been increased by Fe XIX emission, G should be negatively correlated with the above ratio. We find no such correlation. Table 2 shows significant variations in G for both O VII and Ne IX. The quoted errors are due to counting statistics only.

In Figures 3 and 4 we plot lnG vs $s(\theta)$ for O VII and Ne IX, respectively, omitting points for which $\theta \gtrsim 90°$. Table 2 shows that the omitted points have large τ, as expected. Equation (4) shows that $s(\theta)$ depends on an assumed value for Δr. We assume $\Delta r = 4.5 \times 10^9$ cm, which is equal to the scale height, $kT/m_H g_\theta$, where g_θ is the.
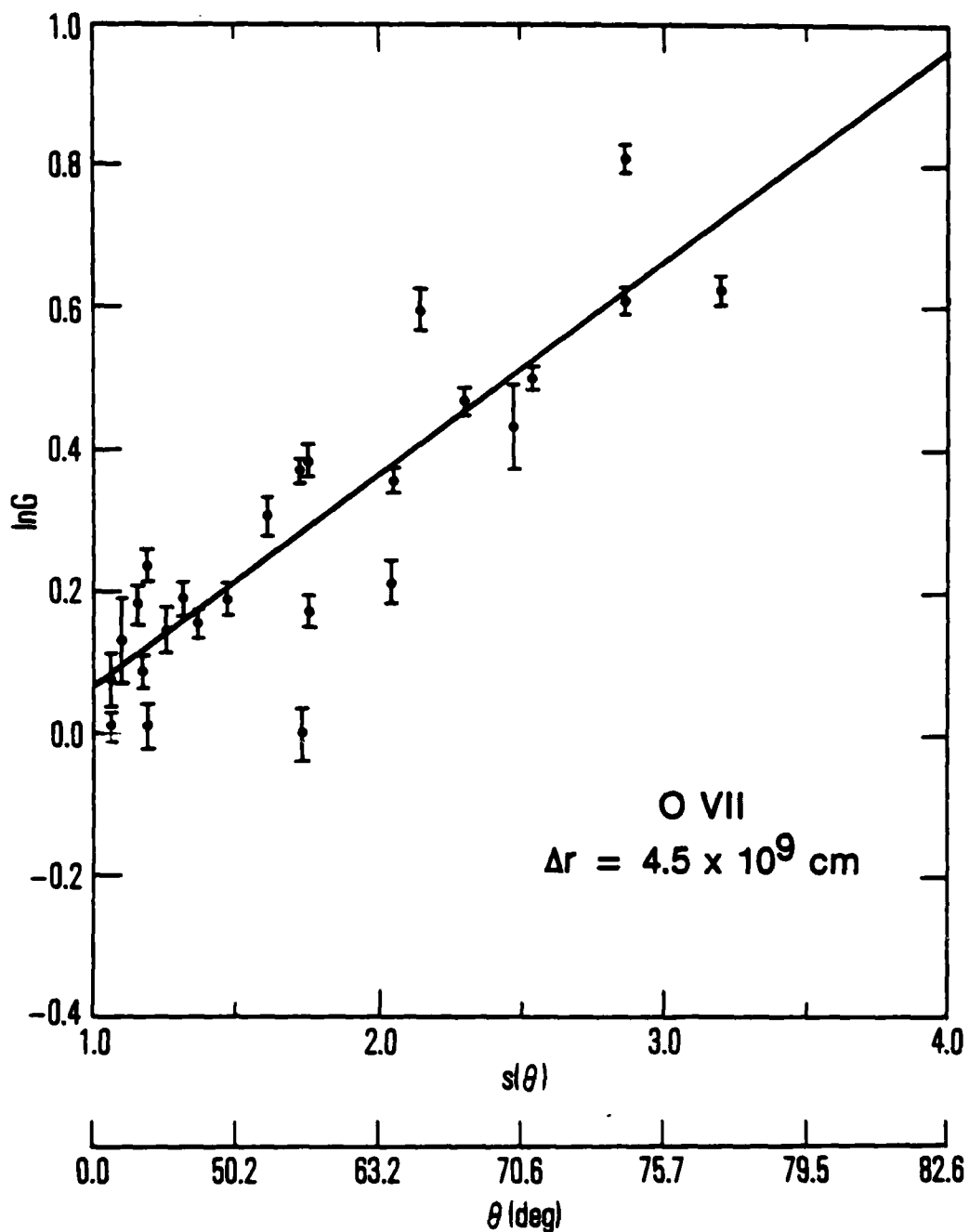
Figure 3. Plot of lnG vs. s(θ) for O VII Observations of Solar
Active Regions. The optical depth for resonance scatter-
ing is proportional to s(θ) (see text). The scale at the
bottom allows G to be related to θ, the angle between the
line of sight and the inward normal to the solar surface.
For θ < 50.2°, s(θ) ≈ sec θ.

29

Figure 4.   Plot of lnG vs. s(θ) for Ne IX.

30
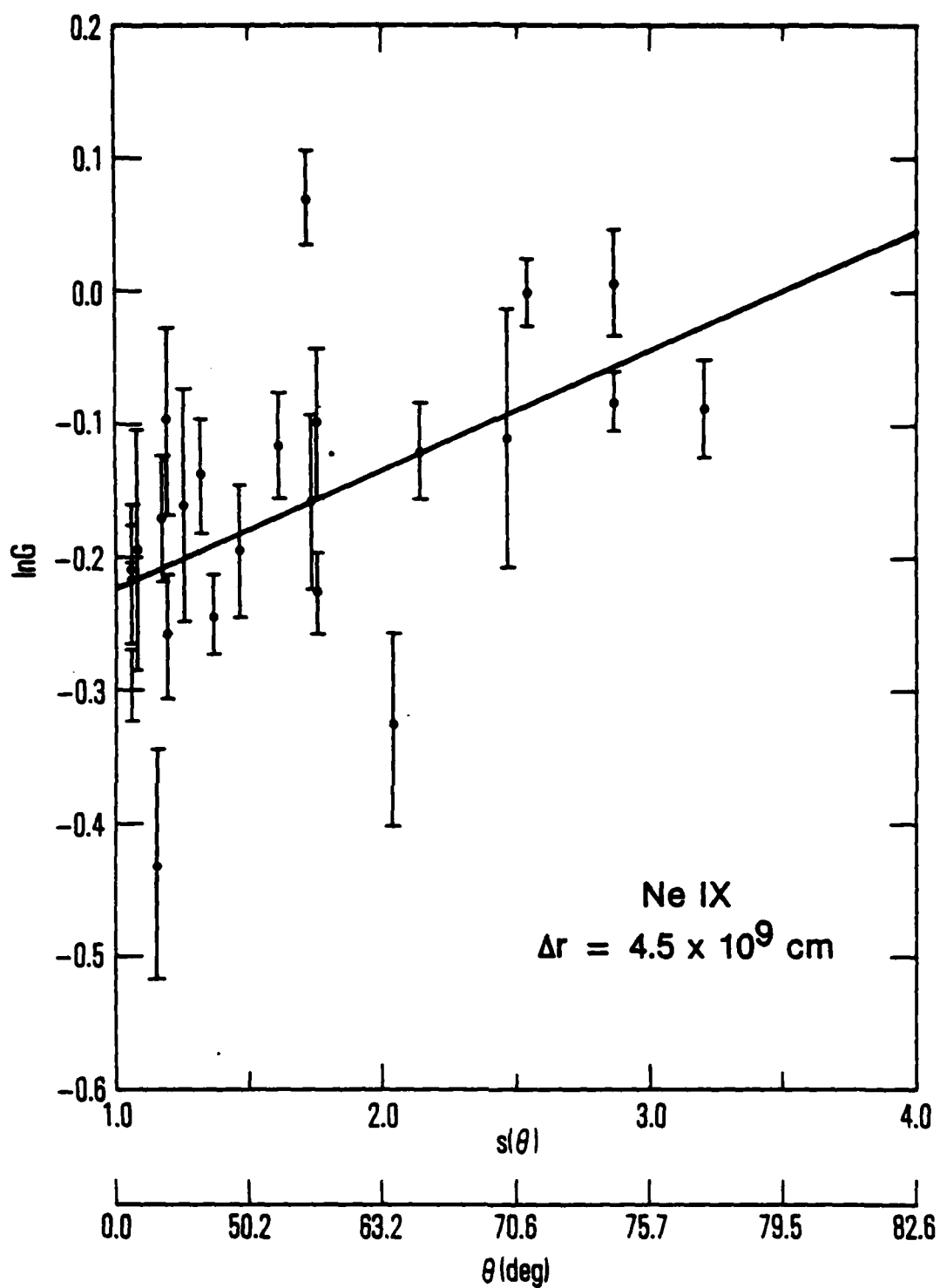
acceleration of gravity at the Sun's surface, m_H is the proton mass, and $T = 1.5 \times 10^6$ K. The results of the analysis below depend weakly on Δr. The best fits to equation (6) are also shown in the figures. Considerable scatter, arising from the inhomogeneity of the corona, is evident.

The curves in Figures 3 and 4 have slope

$$b = \int_{z_s}^{\infty} \kappa(z)dz \ . \tag{7}$$

Acton (1978) gives the following expression for $\kappa_o(z)$ the line center absorption coefficient:

$$\kappa_o(z) = 9.31 \times 10^{-18} \, f_{1u} \, A_i \, A_Z \, n_e(z)\lambda \left(\frac{M}{T_6(z)}\right)^{1/2} \text{cm}^{-1}. \tag{8}$$

In equation (7) f_{1u} is the absorption oscillator strength, A_Z is the element abundance relative to hydrogen, A_i is the fractional population of O VII or Ne IX, λ is the wavelength in Å, M the ion mass in atomic mass units and T_6 the temperature in units of 10^6 K. The effective absorption coefficient, derived by taking the line shapes into account, is $\eta\kappa_o(z)$, where

$$\eta = \left(1 + \frac{T_\epsilon}{T_\alpha}\right)^{-1/2} \tag{9}$$

31

and T_ϵ and T_α are the temperatures in the emitting and absorbing regions, respectively.

The curves can be used to evaluate the electron column densities in the quiet corona and a "typical" active region. We assume that the quiet coronal temperature, T_Q, is 1.5×10^6 K (McKenzie et al. 1978; if $T_Q = 1.0 \times 10^6$ K the results below would be changed very little) and that the active region temperature is 2.5×10^6 K. A_{Ne} is assumed to be 6×10^{-5} and A_O is taken to be 3×10^{-4}. These values are based on Acton's (1978) recommendation that Withbroe's (1976) O abundance be multiplied by 0.65 and on the A_O/A_{Ne} ratio of Acton, Catura, and Joki (1975). Taking $b_O = 0.290$ and $b_{Ne} = 0.090$ from Figures 3 and 4, respectively, we can solve for the electron column densities, N_Q and N_A, in the quiet corona and the typical active region (for $\theta = 0$). We find $N_Q = 3 \times 10^{18}$ cm^{-2} and $N_A = 5 \times 10^{18}$ cm^{-2}. The total column density through the active region is $\sim 2N_A$. With a typical loop height of 2×10^9 cm (Pallavicini et al. 1981) the average active region density is $\sim 5 \times 10^9$ cm^{-3}. If we estimate the quiet coronal path length as the scale height, $kT/m_H g_\odot$, we have n_e at the base of the quiet corona $\sim 7 \times 10^8$ cm^{-3}. Thus the active region density is approximately an order of magnitude higher than that in the quiet corona. With these values, less than $\sim 5\%$ of the O VII emission and less than $\sim 0.5\%$ of the Ne IX emission arise from outside the active region. Approximately 80% of the O VII absorption and $\sim 40\%$ of the Ne IX absorption take place in the quiet corona.

If scattering into the detector could be neglected, G_o could be found by extrapolating the curves in Figures 3 and 4 to $s(\theta)= 0$ (i.e., to $\tau = 0$). However, scattering into the detector is not negligible. Its importance relative to scattering out depends on geometrical relationships between the emitting material and the instrument field of view. Scattering is least important for $\theta = 0$. Judging from sample calculations, raster maps that give us geometrical information, and G values for small θ, we estimate that G_o (O VII) = 1.0 ± 0.1. For Ne IX, G_o can be estimated from $G(\theta \approx 0)$ since Ne IX scattering is almost negligible when θ is small. An average of data from spectra 6-11 and 25-26 with data weighted by σ^{-2} (from Table 2) gives G_o(Ne IX) = 0.80 ± 0.05. The estimated G_o (O VII) agrees with Pradhan and Shull's (1981) calculated value of 1.00, but our G_o(Ne IX) differs substantially from their value of 1.05.

IV. DISCUSSION

The O VII line ratio, R, can be used, as in equation (2), to measure electron densities in the solar corona at $T \approx 2 \times 10^6$ K. Uncertainties in n_e arise from uncertainties in R and in R_o. Errors in R_o are particularly important near the threshold density for which the ratio is applicable. Dividing equation (2) by equation (3) gives, for the uncertainty arising from ΔR_o alone,

$$\frac{\Delta n_e}{n_e} = \frac{\Delta R_o}{R_o - R} \quad , \qquad (10)$$

33

where Δ denotes "uncertainty in." In flares, usually, $\Delta R_0 < < R_0 - R$ (McKenzie et al. 1980a; Doschek et al. 1981), so the uncertainty in R_0 is unimportant. In nonflaring spectra, ΔR_0 is frequently comparable to $R_0 - R$, and uncertainties in n_e are consequently large. A major aim of the study described here has been to evaluate R_0.

From the analysis of 29 O VII spectra, we find that the data are consistent with $R_0 > 3.74$. Correction for blended satellite lines would reduce this lower limit by ~ 1%. We have implicitly assumed that, for our measurements, $T = T_m$. It is likely that there was a small variation in temperature among the various observed regions. We estimate that R_0 varied by ~ 3% (1σ). The R_0 range we arrive at can be considered to be applicable to nonflare spectra. During flares R_0 might be higher, but densities are usually high enough that uncertainties in R_0 do not result in major errors in n_e. We recommend that the same value of R_0 be used in analyzing all O VII data.

In making the density determinations in Table 1 we assumed $R_0 = 3.9 \pm 0.2$. Uncertainties in R and in R_0 were taken into account. Our data allow R_0 as low as 3.7, and all of the data that we know of are consistent with $R_0 \leq 4.1$. Although the uncertainty in R_0 is small, ~ 5%, the uncertainties in n_e in Table 1 are large. In only one case, spectrum 28, is $\Delta n_e / n_e < 0.4$, and in this case the region observed may have been flaring. However, even a density determination with ~ 50% uncertainty may be valuable in studying the physics of coronal active regions.

The attenuation of resonance line flux by resonance scattering is apparent for both O VII and Ne IX. In fact it appears that the O VII flux is almost always subject to significant attenuation. The resonance line flux alone has limited usefulness even in deducing emission measure. Where resonance line flux alone is available, it should be corrected by multiplying it by G/G_o, where G is determined from Figure 3 as a function of θ and $G_o = 1.0$. For Ne IX, resonance scattering in the emitting region is as important as in the intervening corona. This makes it more difficult to correct the Ne IX flux for resonance absorption. On the other hand, since resonance scattering is relatively weak for Ne IX, the use of the curve in Figure 4 in correcting the resonance line flux will usually limit errors to < 20%. Such errors are not serious, given the current state of absolute X-ray spectrometry of the solar corona.

Our interest in G was motivated by its potential usefulness as an indicator of the state of ionization equilibrium of the emitting plasma. Because of resonance scattering, a single measurement of G is inadequate to determine whether or not the plasma is in ionization equilibrium. However, for O VII the resonance scattering takes place primarily in the corona between the source and the observer. This is probably especially true for flares, where the temperature is high and the O VII population is relatively low. If a preflare determination of G is available and the flare values are unchanged, this can be taken as evidence that large departures from ionization equilibrium are not occurring. We have analyzed only a few flares for which

35

preflare G's are available, but in no case have we observed a significant variation in G during a flare. This result is in accord with the conclusion of Doschek, Feldman, and Cowan (1981) that the high-temperature plasmas, from which Fe XXII - Fe XXV lines are emitted, are in ionization equilibrium.

REFERENCES

Acton, L. W. 1978, Ap. J., 225, 1069.

Acton, L. W., and Brown, W. A. 1978, Ap. J., 225, 1065.

Acton, L. W., and Catura, R. C. 1976, Phil. Trans. Roy. Soc. London A, 281, 383.

Acton, L. W., Catura, R. C., and Joki, E. G. 1975, Ap. J. (Letters), 195, L93.

Acton, L. W., Catura, R. C., Meyerott, A. J., Wolfson, C. J., and Culhane, J. L. 1972, Solar Phys., 26, 183.

Bhalla, C. P., Gabriel, A. H., and Presnyakov, L. P. 1975, M. N. R. A. S., 172, 359.

Blumenthal, G. R., Drake, G. W. F., and Tucker, W. H. 1972, Ap. J., 172, 205.

Bromage, G. E., and Fawcett, B. C. 1977, M. N. R. A. S., 178, 591.

Doschek, G. A., Feldman, U., and Cowan, R. D. 1981, Ap. J., 245, 315.

Doschek, G. A., Feldman, U., Landecker, P. B., and McKenzie, D. L. 1981, Ap. J., 249, 372.

Finn, G. D., and Mugglestone, D. 1965, M. N. R. A. S., 129, 221.

Gabriel, A. H., and Jordan, C. 1969, M. N. R. A. S., 145, 241.

_____. 1972, in Case Studies in Atomic Collision Physics, Vol. 2, ed. E. W. McDaniel and M. R. C. McDowell (Amsterdam: North-Holland), p. 209.

Jacobs, V. L., Davis, J., Kepple, P. C., and Blaha, M. 1977, Ap. J., 211, 605.

Jacobs, V. L., Davis, J., Rogerson, J. E., and Blaha, M. 1978, _J. Quant. Spectrosc. Rad. Transf._, 19, 591.

Landecker, P. B., McKenzie, D. L., and Rugge, H. R. 1979, _Proc. Soc. Photo-Opt. Instrum. Eng._, 184, 285.

Mason, H. E., Doschek, G. A., Feldman, U., and Bhatia, A. K. 1979, _Astr. Ap._, 73, 74.

McKenzie, D. L., Broussard, R. M., Landecker, P. B., Rugge, H. R., Young, R. M., Doschek, G. A., and Feldman, U. 1980a, _Ap. J. (Letters)_, 238, L43.

McKenzie, D. L., and Landecker, P. B. 1981, _Ap. J._, 248, 1117.

_____. 1982, _Ap. J._, 254, 309.

McKenzie, D. L., Landecker, P. B., Broussard, R. M., Rugge, H. R., Young, R. M., Feldman, U., and Doschek, G. A. 1980b, _Ap. J._, 241, 409.

McKenzie, D. L., Rugge, H. R., Underwood, J. H., and Young, R. M. 1978, _Ap. J._, 221, 342.

Pallavicini, R., Peres, G., Serio, S., Vaiana, G. S., Golub, L., and Rosner, R. 1981, _Ap. J._, 247, 692.

Pradhan, A. K. 1981 private communication.

Pradhan, A. K., Norcross, D. W., and Hummer, D. G. 1981, _Ap. J._, 246, 1031.

Pradhan, A. K., and Shull, J. M. 1981, _Ap. J._, 249, 821.

Rosner, R., Tucker, W. H., and Vaiana, G. S. 1978, _Ap. J._, 220, 643.

Rugge, H. R., and Walker, A. B. C., Jr. 1970, _Solar Phys._, 15, 372.

_____. 1971, _Solar Phys._, 18, 244.

Serio, S., Peres, G., Vaiana, G. S., Golub, L., and Rosner, R. 1981,
Ap. J., 243, 288.

Withbroe, G. L. 1976, Center for Astrophysics Preprint, 524.

LABORATORY OPERATIONS

The Laboratory Operations of The Aerospace Corporation is conducting exper-
imental and theoretical investigations necessary for the evaluation and applica-
tion of scientific advances to new military space systems. Versatility and
flexibility have been developed to a high degree by the laboratory personnel in
dealing with the many problems encountered in the nation's rapidly developing
space systems. Expertise in the latest scientific developments is vital to the
accomplishment of tasks related to these problems. The laboratories that con-
tribute to this research are:

Aerophysics Laboratory: Launch vehicle and reentry aerodynamics and heat
transfer, propulsion chemistry and fluid mechanics, structural mechanics, flight
dynamics; high-temperature thermomechanics, gas kinetics and radiation; research
in environmental chemistry and contamination; cw and pulsed chemical laser
development including chemical kinetics, spectroscopy, optical resonators and
beam pointing, atmospheric propagation, laser effects and countermeasures.

Chemistry and Physics Laboratory: Atmospheric chemical reactions, atmo-
spheric optics, light scattering, state-specific chemical reactions and radia-
tion transport in rocket plumes, applied laser spectroscopy, laser chemistry,
battery electrochemistry, space vacuum and radiation effects on materials, lu-
brication and surface phenomena, thermionic emission, photosensitive materials
and detectors, atomic frequency standards, and bioenvironmental research and
monitoring.

Electronics Research Laboratory: Microelectronics, GaAs low-noise and
power devices, semiconductor lasers, electromagnetic and optical propagation
phenomena, quantum electronics, laser communications, lidar, and electro-optics;
communication sciences, applied electronics, semiconductor crystal and device
physics, radiometric imaging; millimeter-wave and microwave technology.

Information Sciences Research Office: Program verification, program trans-
lation, performance-sensitive system design, distributed architectures for
spaceborne computers, fault-tolerant computer systems, artificial intelligence,
and microelectronics applications.

Materials Sciences Laboratory: Development of new materials: metal matrix
composites, polymers, and new forms of carbon; component failure analysis and
reliability; fracture mechanics and stress corrosion; evaluation of materials in
space environment; materials performance in space transportation systems; anal-
ysis of systems vulnerability and survivability in enemy-induced environments.

Space Sciences Laboratory: Atmospheric and ionospheric physics, radiation
from the atmosphere, density and composition of the upper atmosphere, aurorae
and airglow; magnetospheric physics, cosmic rays, generation and propagation of
plasma waves in the magnetosphere; solar physics, infrared astronomy; the
effects of nuclear explosions, magnetic storms, and solar activity on the
earth's atmosphere, ionosphere, and magnetosphere; the effects of optical,
electromagnetic, and particulate radiations in space on space systems.